Algorithm Theoretical Basis Document for Global Coastal Upwelling Index from EOS-06 (OCEANSAT-3) Scatterometer

S. No.	Product Name	Spatial Resolution (km)	Temporal Resolution
1	EO6SCTL4UI_YYYYDDD_25km.nc	25X25	Daily

Debojyoti Ganguly and K. N. Babu

Biological Oceanographic Division

Atmospheric and Oceanic Sciences Group

Space Applications Centre, ISRO

Ahmedabad 380015, India

1. Algorithm Configuration Information

1.1 Algorithm Name

Automatic Coastal Upwelling Estimation.

1.2 Algorithm Identifier

EO6SCTL4UI_YYYYDDD_25km.nc

1.3 Algorithm Specification

Version	Date	Prepared by	Description
1.0.0	22/11/2024	Debojyoti Ganguly and K.N. Babu	Estimation of coastal upwelling index on an automated basis for global coast.

Introduction

Wind stress is an important forcing of sea surface perturbations, as either waves or sea surface currents (Wang et al. 2010). Upwelling is an oceanographic phenomenon that involves wind-driven motion of dense, cooler, and usually nutrient-rich water towards the ocean surface, replacing the warmer, nutrient depleted surface water (Smitha et al. 2008). Upwelling zones are among the most productive regions of the world's oceans (Bakun et al 2010). They are characterized by alongshore coastal winds that push water offshore and thus pump (i.e. 'upwell') nutrient rich deeper waters into the sunlit surface layers where they are available for photosynthesis. The coastal upwelling regions of the world support some of the most diverse ecosystems like the Peruvian anchovy and are also prominent fishing zones. It has been reported that even though the coastal upwelling regions occupy less than 2 percent of the global ocean, they constitute more than 20 percent of the global fish catch. This is because the coastal upwelling regions are highly productive oceanic ecosystems. Any change in coastal winds and upwelling characteristics can affect the coastal marine ecosystem and thus it is necessary to examine the strength and intensity of upwelling.

Upwelling occurs along a coastline when surface wind stress produces offshore Ekman transport or wind stress curl produces upward motion at the bottom of the Ekman layer. Ekman transport is the process by which alongshore winds displace the surface waters away from the coast which is then replaced by water from the base of Ekman layer. Coastal upwelling regions comprise of western boundary and eastern boundary upwelling systems. Some of the most prominent eastern boundary upwelling systems include the Peru upwelling, Benguela upwelling, California and Canary upwelling. Somalia and Oman upwelling are the two major western boundary upwelling systems. In eastern boundary upwelling like Peru and Benguela equatorial trade winds sustain upwelling activity almost all round the year resulting in high primary productivity. In Oman and Somalia upwelling strong alongshore winds during the south west monsoon months of June to September drive coastal upwelling. In this Algorithm Theoretical Basis Document (ATBD) an automated method for estimation of coastal upwelling index on a daily basis using Oceansat-3 scatterometer wind data has been demonstrated. This method computes the coastal upwelling index up to a distance of 300 km from the coast on a global scale.

Oceansat-3

Oceansat-3 is a follow on mission to ISRO's Oceansat series of satellites which was launched on 26 November 2022 from Satish Dhawan Space Centre, Shriharikota. It is designed to provide continuity of ocean colour measurements over Indian and global oceans in 13 channels in Visible-Near InfraRed (VNIR). Apart from Ocean Colour Monitor (OCM-3), Oceansat-3 also has Sea Surface Temperature Monitor (SSTM) and a Ku band (13.5 Ghz) scatterometer, OSCAT-3 for near surface winds over global oceans. Unfortunately SSTM developed a problem soon after launch and ceased functioning.

Overview and Background

Upwelling indices are used to denote the strength and intensity of coastal upwelling. Any change in upwelling characteristics like upwelling intensity and duration can affect the coastal ecosystem. Long term time series of upwelling indices can provide crucial insights into how coastal upwelling systems are evolving in a global warming scenario. The Bakun Index is one of the most commonly used upwelling index. It uses available estimates of atmospheric conditions and Ekman theory to derive estimates of cross-shore Ekman transport as a proxy for coastal upwelling. Some upwelling indices use the Sea surface temperature as a proxy for upwelling. The temperature difference between the coastal waters and offshore waters can be a reliable proxy for upwelling strength. In this document we discuss the Bakun Index and its implementation on daily scatterometer wind data.

In some coastal areas of the ocean and large lakes like the North American great Lakes, the combination of persistent winds, Earth's rotation (Coriolis effect), and restrictions on lateral movements of water due to shorelines induces upward and downward water movements. Ekman transport and Ekman pumping are the two mechanisms that induce upwelling and downwelling in oceans. Ekman transport is the net motion of fluid as a result of a balance between Coriolis and turbulent drag force induced by surface wind stress. Ekman transport was first investigated by Vagn Walfrid Ekman in 1902 who used the term Ekman spiral to denote the movement of subsurface water dragged by wind stress. When surface water molecules move by the force of wind, they in turn drag deeper layers of water molecules below them. Each layer of water molecules is moved by friction from the shallower layer and each deeper layer moves more slowly than the layer above it. The resultant movement in the Ekman layer is a spiral referred as Ekman spiral.

Upwelling in the ocean can be due to uniform alongshore winds or spatially varying wind fields having a positive curl or due to both. The alongshore winds impart a stress on the surface of ocean which depends on the wind speed and a drag coefficient. Firstly, the wind stress is computed from the bulk aerodynamic formula as used for satellite derived wind stresses by Koracin et al. 2004 and Petit et al. 2006

$$\tau = \rho C_d W^2 \quad (1)$$

Where τ is the wind stress, ρ is the density of air taken as 1.25 kg/m^3, C_d is the wind dependent drag coefficient calculated using the Large and Pond method (1981) and W is the wind speed at 10m height.

The zonal and meridional component of wind stress is computed as

$$\tau_x = \rho C_d W U \quad (2)$$

$$\tau_y = \rho C_d W V \quad (3)$$

Where U and V are the zonal and meridional component of wind speed respectively.

The zonal and meridional component of Ekman mass transport is given as

$$M_x = \frac{\tau_y}{f} \quad (4)$$

$$M_y = -\frac{\tau_x}{f} \quad (5)$$

Where f is the Coriolis parameter ($2\Omega \sin\Phi$), Ω is the angular velocity of the earth and Φ is the latitude in degrees.

For coastal upwelling the Ekman mass transport in a direction perpendicular to the coast is of importance. Thus, the zonal and meridional component of mass transport are converted into alongshore and across shore component of Ekman mass transport using an estimate of the shoreline angle.

Apart from Ekman transport there is another mechanism of upwelling called Ekman pumping and occurs due to the curl of the wind stress. In open ocean areas Ekman pumping is the main driver of upwelling.

The Ekman pumping velocity is calculated as (Pickett et al. 2003 and Smith et al. 1968)

$$v = \frac{\nabla \times \tau}{\rho f} \quad (6)$$

Where v is the Ekman pumping velocity (m/s), τ is the wind stress, ρ is the water density for sea water taken as 1024 kg/m^3 and f is the Coriolis parameter

The offshore component of Ekman mass transport can be used as an index of upwelling.

Pacific Fisheries Environmental Laboratory (PFEL) provides a time series of upwelling index (off-shore component of Ekman transport) for any location along a coastline, given the orientation of the coastline. PFEL provides global upwelling index at 1^0 resolution. However, it needs the coastal angle as input by user along with coastal latitude and longitude input. We evaluate the upwelling indices in a coastal band of approximately 300 km using coastline slope evaluated with high resolution coastal shapefiles.

Algorithm Description

Global shoreline shapefiles are first downloaded from National Oceanic and Atmospheric Administration (NOAA) National Centers for Environmental Information. Geography data are in five resolutions: crude (c), low (l), intermediate(i), high (h), and full (f). Shorelines are organized into four levels: boundary between land and ocean (L1), boundary between lake and land (L2), boundary between island-in-lake and lake (L3), and boundary between pond-in-island and island (L4). We used the L1 level shorelines at low resolution. The low resolution was selected because it was comparable to the spatial resolution of the scatterometer data. The shapefile was structured as multiple polygons each representing a particular continent, country or island.

Firstly an array was created with rows equal to the total number of points including all polygons and columns equal to 4. The first two columns of this array are populated with the latitude and longitude values taken from the coastline polygon shapefiles. The third column of this array has the corresponding coastal angles. The fourth column contains either +1 or -1 and is used to indicate which side the land boundary falls. Since for upwelling estimates we are interested in the component of Ekman transport along the outward normal to shoreline the +- 1 multiplicative factor is used. Coastal angle for each point is computed with respect to the north direction using the latitude and longitude values on both sides of the point and fitting a straight line to the coastal segment. The angle is measured such that it lies between -90 and +90. Angles measured clockwise are positive and anticlockwise are considered negative according to our convention.

For computing the multiplicative factor (+-1), we use the two coastal points from which the coastal angle was computed and obtain its mid-point. We then calculate the slope of the normal using the slope of the coastal segment. A line is then fitted using the computed midpoint and

the slope of the normal. We then compute the latitude and longitude of a point 100 kms on both sides of the normal. One of these points is towards land and the other is towards sea. We assign +1 if the land boundary is towards west (eastern boundary upwelling systems) and assign -1 if the land boundary is towards east (western boundary upwelling systems).

The next step is creating two arrays of the same size as the wind input obtained from scatterometer data and estimating the angle and multiplicative factor at each pixel. For every pixel the nearest coastal point is computed. Pixels which are more than 300 kms away from the nearest coastal point are filled with NaN values. For pixels which are within 300 kms of coast, the nearest coastal point is computed and coastal angle and multiplicative factor for the point are used in the pixel for the two arrays.

The wind input is then used to compute the zonal and meridional component of Ekman transport for each pixel in the scatterometer data using equations 4 and 5. The zonal and meridional component of Ekman mass transport are then used to compute the across-shore component of mass transport using the coastal angle and multiplicative factor using the following equation (Ganguly et al. 2023).

$$M_{offshore} = \pm 1 * (M_x * \cos(\theta) - M_y * \sin(\theta)) \quad (7)$$

Where, $M_{offshore}$ is the offshore Ekman mass transport ($kgm^{-1}s^{-1}$), M_x is the zonal mass transport, M_y is the meridional transport and Θ is the coastal angle. The +- 1 is the multiplication factor to account for the shoreward and seaward side of the coastal point.

The offshore component of Ekman transport is called as upwelling index (UI) and is calculated at the same spatial resolution as the input wind data and is computed up to a distance of 300 kms which is the extent up to which coastal processes occur.

The brief outline of the methodology is presented in the form of a flowchart as shown in Figure 1.

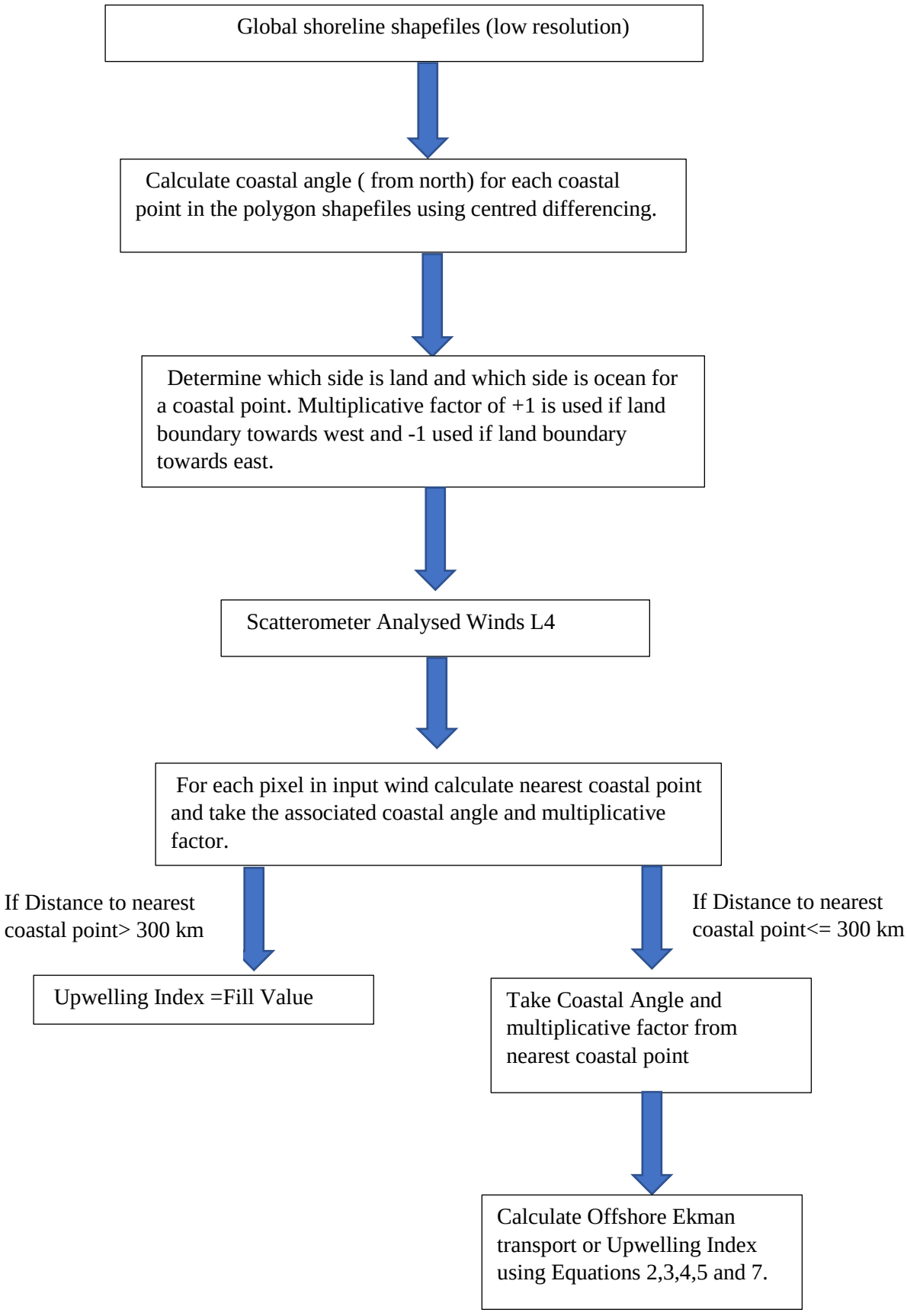

Figure 1: Flowchart of Upwelling Index computation from scatterometer winds

Daily L4 analysed wind data from EOS 06 scatterometer would be used to generate daily global upwelling index product at 25km spatial resolution. It would be of the same size as the input wind and valid upwelling indices at ocean pixels which are within 300 kms away from coast. All other pixels would have fill values.

This method is able to extract coastline slope and offshore Ekman transport automatically. However, this method also estimates UI around very small islands which is undesirable. Even though island nations also have coastal upwelling there is limited ability of 25 km analysed winds from scatterometer to characterize coastal upwelling for small islands which occupy only few pixels in the scatterometer data. For this reason coastal upwelling is not estimated for islands smaller than 40,000 square kilometres. Coastal areas surrounding such islands are populated with fill values.

Results :

Figure 2 shows the daily upwelling index (UI) computed for two different dates in June 2024. Positive values indicate upwelling and negative values indicate downwelling. This month marks the onset of south west monsoon in Indian subcontinent. During this period strong south westerly winds drive coastal upwelling along the Somalia-Oman coast and also along the coasts of India. High UI exceeding 2-3 m^2/s are observed near Oman, Somalia and coastal India during these dates of June 2024. It can be observed that the automatic estimation of global coastal upwelling index is very well able to detect the well known permanent upwelling regions like the Peru upwelling, Benguela upwelling, Canary and California upwelling. It is observed that most coastal areas are neutral with no upwelling or downwelling signatures. The UI for most coastal areas is close to 0 m^2/s and regions with visible upwelling are a very small fraction of total coastal area. This is expected as it has been reported that the upwelling areas comprise less than 2 percent of the global coast. But these areas are very crucial for fisheries as they account for approximately 20 percent of the global fish catch.

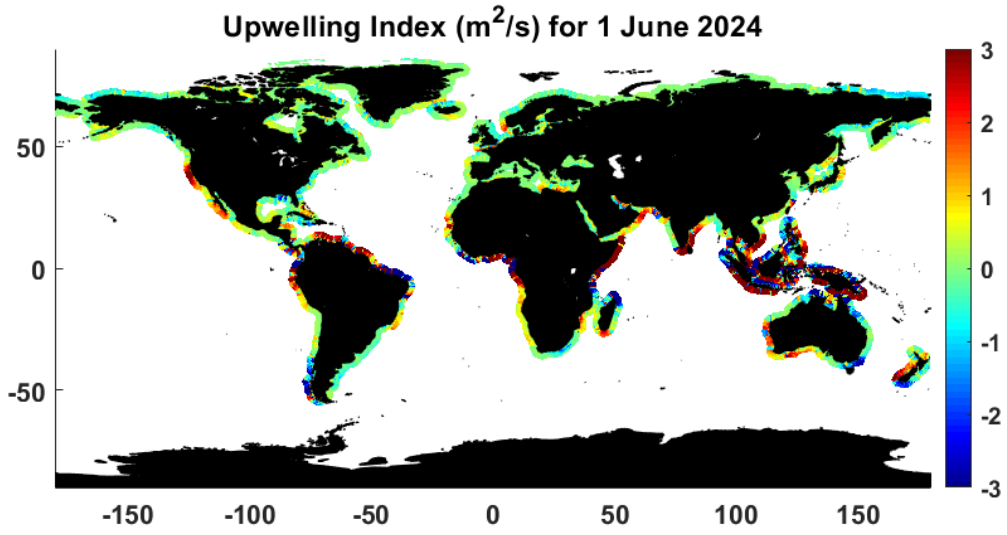

(a)

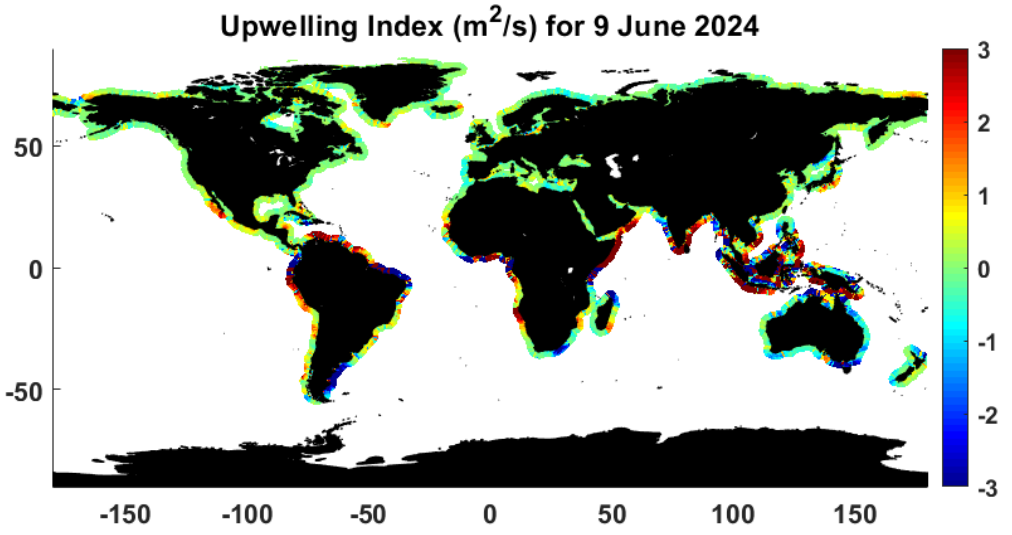

(b)

Figure 2: (a) Upwelling index for 1 June 2024, (b) Upwelling index for 9 June 2024.

Validation and Uncertainty estimates:

A limited validation of the daily upwelling index is carried out. 20 random points are considered in various parts of the global coast and their upwelling index estimated for the above 2 dates. Thus we have a total of 40 data points. These random points are taken so that they cover almost all the well known global upwelling areas. The points are shown in Figure 3.

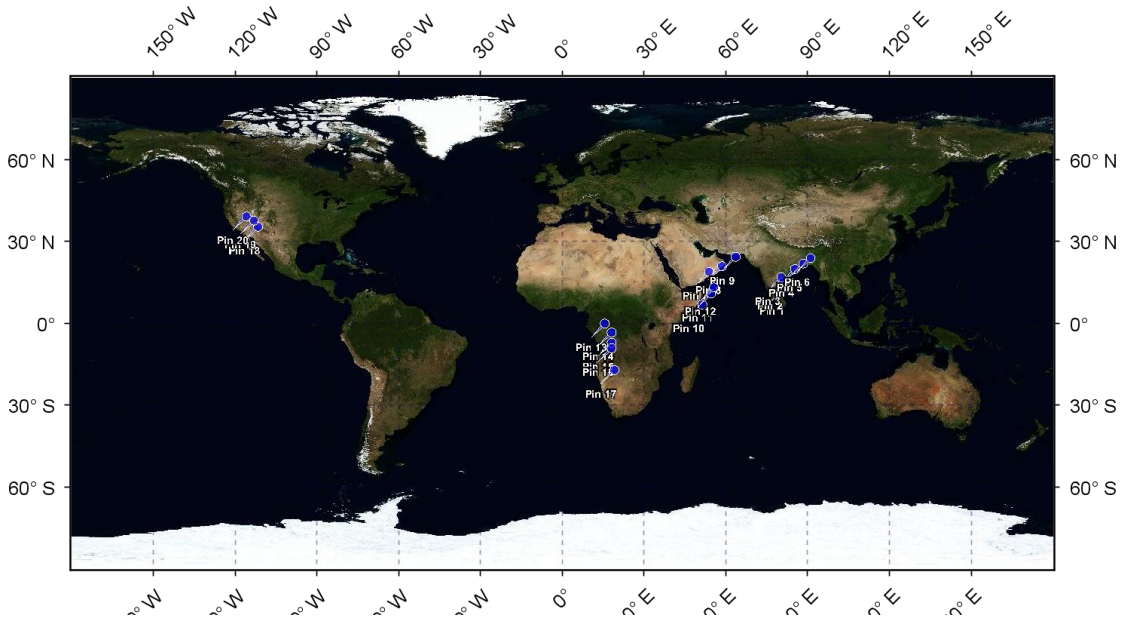

Figure 3: Coastal points over which validation has been performed.

In order to perform the validation exercise the upwelling index is first estimated for the 20 points using the automated upwelling index estimation technique and compared with upwelling estimates using manual method. Since the automated technique extracts coastal orientation as well as outward normal automatically it is a potential source of uncertainty as far as upwelling index is concerned. The most difficult task is determining the outward normal towards the sea for any coastal point. With the manual method we can manually check if the coastline orientation computed for a point is correct or not. However, for the automatic method it is not possible as there are thousands of points for which upwelling index is estimated. The automatic method has to correctly estimate not just the coastal angle but also determine which side is sea and which side is land for any coastal point. If we are unable to resolve this direction ambiguity properly we cannot determine the sign of the upwelling index (positive or negative) even though we may get the magnitude correctly. Another source of error is inability to properly determine coastal orientation for gulf waters, straits and oceanic regions surrounded by landmasses. Since this method determines the closest coastline point and estimates coastline slope it is prone to error for points lying between two different landmasses. The validation scatter and statistics are shown in Figure 4.

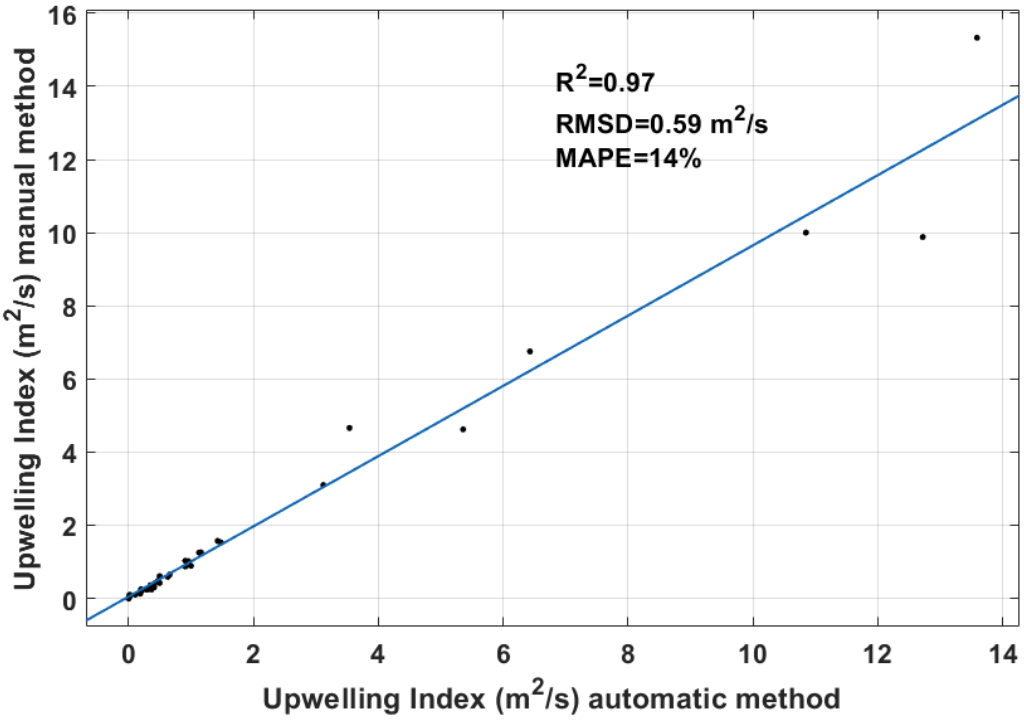

Figure 4: Scatter statistics for Upwelling index

It is observed from Figure 4 that there is very good correlation between both the upwelling index with a coefficient of determination (R^2) of 0.97. The RMSE observed is 0.59 m^2/s which appears a bit high because of some high upwelling index values. The Mean Absolute percentage error (MAPE) is thus estimated as the RMSE appears misleading. The MAPE is defined as

$$MAPE = 100 * \frac{1}{n}\sum_{t=1}^{n}\left|\frac{A_t - F_t}{A_t}\right| \quad (10)$$

Where A_t is the actual value and F_t is the forecast value and n is the number of fitted points.

The MAPE is observed to be 14% which is reasonably good. The equation for upwelling index estimation is standard and are widely used for upwelling index estimation. However, there are different versions of the drag coefficient because of which values of upwelling index can vary between researchers. The simplistic version use a constant value of drag coefficient while recently wind dependent drag coefficients are used for more accurate estimates. The errors in wind speed and wind direction are other likely sources of error in upwelling estimates.

Sensitivity of Coastal Upwelling Index to Wind Speed and Wind Direction:

Uncertainty in coastal wind speed and wind direction are one of the main sources of error as far as coastal upwelling index is concerned. Sensitivity analysis is carried out to show the sensitivity of Upwelling Index with measured wind. Figure 5 shows an illustration of wind blowing at an angle to the coastline. It also shows the direction of outward normal to the coast which is the direction for estimating UI. Figure 6 shows the variation of Upwelling Index with change in wind speed for three different angle between coastline slope and wind direction. It can be seen that as the angle between coastline and wind direction increases, the Upwelling Index decreases. It is maximum when the wind is parallel to the coast and decreases with increasing angle.

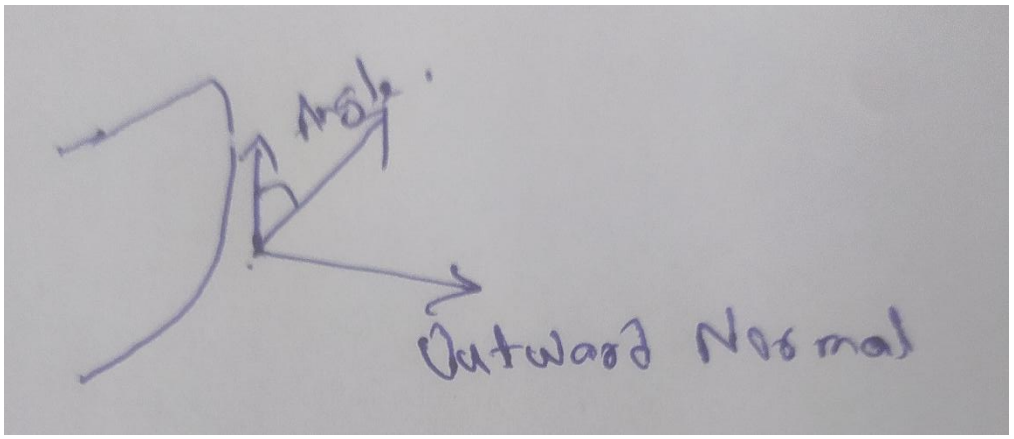

Figure 5: Illustration showing the Angle between wind and coastline and the direction of outward normal to coast.

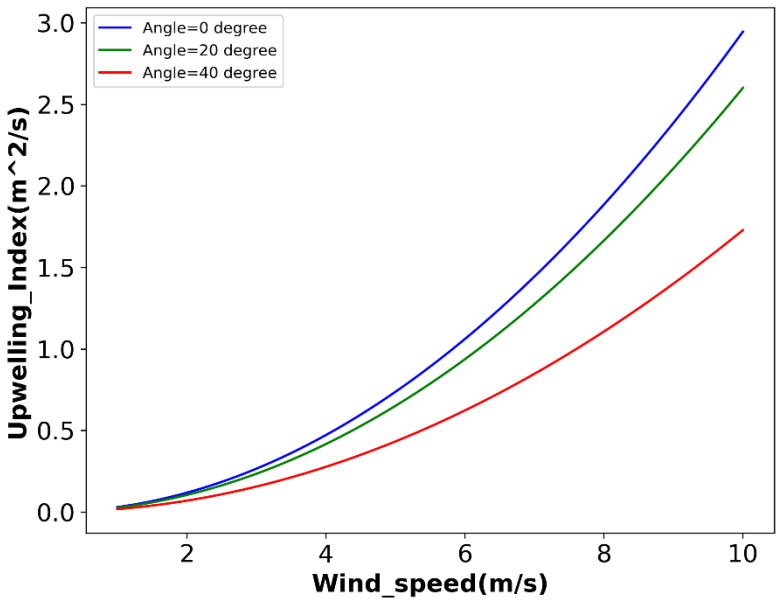

Figure 6: Upwelling Index (m^2/s) variation with wind speed at various angle between coast and wind direction.

Figure 7 shows the variation of UI with wind direction for 3 different wind speed of 5m/s, 6m/s and 7m/s. It can be seen that the upwelling index is maximum when the angle between coast and wind is 0 degrees and is in mimimum with negative magnitude when the angle is 180 degrees. It can also be seen that the slope of the curves is mimimum near 0 degrees, 90 degrees and 180 degrees indicating that UI is less sensitive to errors in wind direction at these angles.

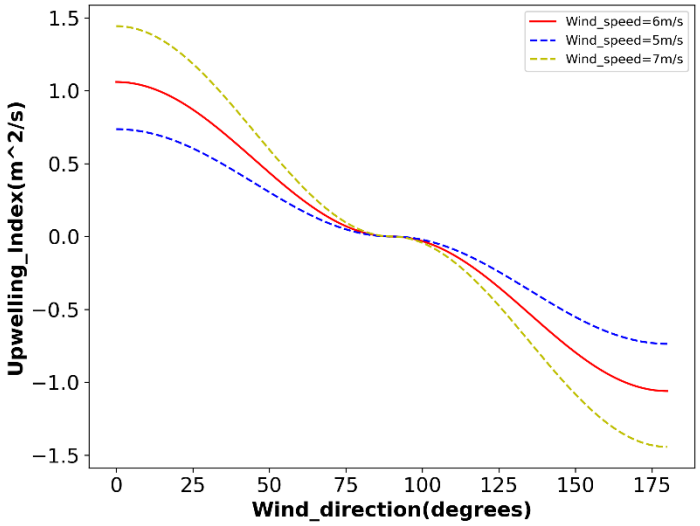

Figure 7: Upwelling Index (m^2/s) variation with wind direction for 3 different wind speed cases.

Conclusion:

An automatic method of coastline slope estimation and daily upwelling index estimation from EOS-06 scatterometer is presented. This method is able to successfully extract coastline orientation on an automatic basis with reasonable fidelity. Validation done with manual estimation of upwelling index shows high correlation demonstrating the potential to automate the method for global scale estimation on a daily basis. More recent formulations of wind dependent drag coefficient could be tested for further improvement. The retrieval and masking around small island nations needs to be investigated properly. Moreover, the challenges in retrieval in enclosed and semi-enclosed seas need to be addressed for improved product quality.

Acknowledgment

We acknowledge Director, Space Applications Centre (ISRO), Ahmedabad for his continuous support for pursuing this study. We are also thankful to Deputy Director, Earth, Ocean, Atmosphere, Planetary Sciences and Applications Area (EPSA), ISRO for keen interest and support in this field. The authors also express their heartfelt gratitude to Meteorological and Oceanographic Satellite Data Archival Centre (MOSDAC) for making L4 Analyzed Wind data available without which this work would have been incomplete.

References:

1) Bakun, A., Field, D.B., Rodriguez, A.R., Weeks, S.J., 2010. Greenhouse gas, upwelling-favorable winds, and the future of coastal ocean upwelling ecosystems. Global Change Biology. 16(4): 1213-1228.
2) Ganguly, D., Suryanarayana, K., Raman, M. 2023. Spatio-temporal variations in upwelling indices in Arabian Sea coastal upwelling systems and associated biological productivity using remote sensing observations. Journal of Operational Oceanography. 17(1):63-76. Doi: 10.1080/1755876X.2023.2186588.
3) Koracin, D., Dorman, C.E., Dever, E.P., 2004. Coastal perturbations of marine-layer winds, wind stress and wind stress curl along California and Baja California in June 1999. Journal of Physical Oceanography. 32: 1152-1173. doi: 10.1175/1520-0485(2004)034<1152:CPOMWW>2.0.CO;2.
4) Large WG, Pond S. 1981. Open ocean momentum flux measurements in moderate to strong winds. Journal of Physical Oceanography. 11: 324-336. doi: 10.1175/1520-0485(1981)011<0324:OOMFMI>2.0.CO;2.
5) Petit M, Ramos AG, Lahet F, Copa J. 2006. Satellite - derived ERS Scatterometer - sea surface wind stress curl in the southwestern Indian Ocean. Geoscience. 338 (3): 206-213. doi: 10.1016/j.crte.2005.10.002.
6) Pickett MH, Paduan JD. 2003. Ekman transport and pumping in the California Current based on the U.S. Navy's high resolution atmospheric model (COAMPS). Journal of Geophysical Research: Oceans. 108(C10), 3327. doi: 10.1029/2003JC001902.
7) Smitha BR, Sanjeevan VN, Vimalkumar KG, Revichandran C. 2008. On the upwelling off the southern tip and along the west coast of India. Journal of Coastal Research. 24(3): 95-102. doi: 10.2112/06-0779.1.

8) Smith RL. 1968. Upwelling, Oceanography and Marine Biology*:* An Annual Review. 6: 11-46.

9) Wang Q, Kalogiros J.A. Ramp S.R. 2011. Wind Stress Curl and Coastal Upwelling in the Area of Monterey Bay Observed during AOSN-II. Journal of Physical Oceanography. 41: 857-877. doi: 10.1175/2010JPO4305.1.